Eur. Phys. J. B **7**, 53–66 (1999)

THE EUROPEAN PHYSICAL JOURNAL B

EDP Sciences

Photoemission, inverse photoemission and superconducting correlations in Hubbard and t–J ladders: role of the anisotropy between legs and rungs

J. Riera[1,2], D. Poilblanc[1,a], and E. Dagotto[3]

[1] Laboratoire de Physique Quantique[b], Université Paul Sabatier, 31062 Toulouse, France
[2] Instituto de Física Rosario, Consejo Nacional de Investigaciones Científicas y Técnicas y Departamento de Física, Universidad Nacional de Rosario, Avenida Pellegrini 250, 2000-Rosario, Argentina
[3] Department of Physics and National High Magnetic Field Lab, Florida State University, Tallahassee, FL 32306, USA

Received: 22 April 1998 / Revised: 23 July 1998 / Accepted: 30 July 1998

Abstract. Several experiments in the context of ladder materials have recently shown that the study of simple models of anisotropic ladders (*i.e.* with different couplings along legs and rungs) is important for the understanding of these compounds. In this paper Exact Diagonalization studies of the one-band Hubbard and $t-J$ models are reported for a variety of densities, couplings, and anisotropy ratios. The emphasis is given to the one-particle spectral function $A(\mathbf{q},\omega)$ which presents a flat quasiparticle dispersion at the chemical potential in some region of parameter space. This is correlated with the existence of strong pairing fluctuations, which themselves are correlated with an enhancement of the bulk-extrapolated value for the two-hole binding energy as well as with the strength of the spin-gap in the hole-doped system. Part of the results for the spectral function are explained using a simple analytical picture valid when the hopping along the legs is small. In particular, this picture predicts an insulating state at quarter filling in agreement with the metal–insulator transition observed at this special filling for increasing rung couplings. The results are compared against previous literature, and in addition pair-pair correlations using extended operators are also here reported.

PACS. 71.27.+a Strongly correlated electron systems; heavy fermions – 74.72.-h High-T_c compounds – 75.40.Mg Numerical simulation studies – 79.60.-i Photoemission and photoelectron spectra

1 Introduction

The discovery of superconductivity in quasi-two dimensional (2D) copper-oxide materials has led to a renewed interest in the physics of doped Mott-Hubbard insulators and in the interplay between magnetism and superconductivity. Recently another class of copper oxide materials based on weakly coupled one dimensional (1D) ladders [1] has been synthetised. Their structure is closely related to the one of the 2D perovskites, namely it contains $S = 1/2$ copper spins which are antiferromagnetically coupled along the ladder direction (legs) and along the rungs through Cu–O–Cu bonds. Recent experimental results reporting superconductivity [2] in the hole-doped ladder cuprate $Sr_{14-x}Ca_xCu_{24}O_{41}$ have clearly established that the existence of a superconducting state is not restricted to 2D doped antiferromagnets but it actually extends to a wider class of strongly correlated copper-oxide materials. Thus, the novel ladder compounds offer new perspectives, both for experimentalists and theorists, to understand the mechanism of superconductivity in strongly correlated low-dimensional systems.

Ladder structures can also be found in other oxides such as vanadates [3]. Magnetic susceptibility measurements on MgV_2O_5 have been interpreted in terms of weakly coupled Heisenberg ladders. In addition, recent X-rays scattering experiments [4] have suggested that NaV_2O_5 could be considered as a quarter-filled ladder system.

While the stoichiometric parent compounds of the superconducting 2D cuprates are antiferromagnetic Mott insulators, the parent insulating ladders exhibit spin liquid properties. The existence of a spin gap in a spin-ladder structure has been first proposed theoretically [5,6] and found experimentally in several even-leg ladder copper-oxide systems (such as $SrCu_2O_3$ [1,7] and $LaCuO_{2.5}$ [8]).

It has been suggested that the spin gap, if robust under doping, could be responsible for an attractive interaction between holes on the same rung [6,9]. Although recent experiments [10] suggest that the spin gap

[a] e-mail: didier@irsamc2.ups-tlse.fr
[b] CNRS – UMR 5626

disappears in hole-doped ladders at the high pressure needed to achieve superconductivity, part of the spin excitations are still suppressed as the temperature is lowered in the normal state as predicted theoretically [11]. Such a behavior bears similarities with the pseudogap behavior of the underdoped 2D superconducting cuprates.

It is expected that the formation of hole pairs on the rungs can lead to competing superconducting pairing or $4k_F$ Charge Density Wave (CDW) correlations as *e.g.* found in the weak coupling limit [12,13]. For isotropic $t-J$ ladders (*i.e.* with equal couplings along legs and rungs), it has been established that the d-wave-like superconducting pairing correlations [14] are dominant in a large region of the phase diagram [15]. Such a state, which is referred to as $C1S0$ in the language of the RG analysis [16], is characterized by a single gapless charge mode and a gap in the spin excitation spectrum [11] and belongs to the same universality class as the Luther-Emery phase of the 1D chain. Because of the one-dimensional character of the system, the superconducting correlations at large distances still behave following power laws [13,15]. Using finite size scaling analysis and conformal invariance relations [15], the corresponding critical exponents have been computed in the case of equal rung and leg couplings (isotropic case). Note that a small Josephson tunneling between the ladders is expected to give a finite superconducting critical temperature [17]. At finite doping, the spin gap is expected to vanish below a small critical J/t ratio [15,18]. Presumably, such a transition is associated to an instability of the hole pairs gas towards a liquid made out of individual holes with two spin and two charge collective modes ($C2S2$ phase) [18]. Whether the disappearance of the spin gap observed by NMR experiments in the doped $Sr_{14}Cu_{24}O_{41}$ superconducting ladder material under pressure [10] is connected to such a transition is under much debate.

Although the isotropic case is the most widely analyzed situation in the context of theories for ladders, it has now become clear that most of the actual ladder materials have in fact different leg ($J_\parallel$) and rung ($J_\perp$) magnetic couplings and/or hopping matrix elements $t_\parallel$ (legs) and $t_\perp$ (rungs). Recent neutron scattering experiments [19] on the insulating ladder $Sr_{14}Cu_{24}O_{41}$ actually suggest a ratio of $J_\perp/J_\parallel \simeq 0.5$. A similar anisotropy was in fact also predicted previously in the context of the $SrCu_2O_3$ material [20]. On the other hand, the vanadate ladder NaV_2O_5 apparently corresponds to the opposite limit of strong rung couplings with a ratio $t_\perp/t_\parallel \simeq 2$ [21] which could justify a description at quarter-filling in terms of an effective 1D Heisenberg model [21,22].

The purpose of the present paper is to investigate spectral properties and superconducting correlations of anisotropic Hubbard and $t-J$ ladders by exact diagonalization methods. Finite size scaling analysis is used to obtain physical quantities such as the pair binding energy or the spin gap. Dynamical correlations functions are also computed using a continued fraction method. The focus of the paper will be on the role of the ladder anisotropy (regulated by the ratios of the rung couplings to the leg couplings) as well as on the influence of doping. The anisotropic Hubbard ladder is defined as,

$$\begin{aligned} H = & t_\parallel \sum_{i,\alpha,\sigma} (c^\dagger_{i,\alpha;\sigma} c_{i+1,\alpha;\sigma} + h.c.) \\ & + t_\perp \sum_{i,\sigma} (c^\dagger_{i,1;\sigma} c_{i,2;\sigma} + h.c.) \\ & + U \sum_{i,\alpha} n_{i,\alpha;\uparrow} n_{i,\alpha;\downarrow} \,, \end{aligned} \tag{1}$$

where the index α stands for the chain index ($= 1,2$). Anisotropy ratios $r_a = t_\perp/t_\parallel$ in the range $0.5 \leq r_a \leq 2.5$ will be considered. Most of the calculations reported below have been carried out in the strong coupling regime $U/t_\parallel = 8$. Motivated by the doped cuprate and vanadate ladders, the studies below are performed in the electron density range $0.5 \leq n \leq 1$. For $U/t_\parallel \gg 1$ and $U/t_\perp \gg 1$, the low energy spin and charge degrees of freedom can be described by the effective anisotropic $t-J$ ladder with doubly occupied sites projected out,

$$\begin{aligned} H = & J_\parallel \sum_{i,\alpha} (\mathbf{S}_{i,\alpha} \cdot \mathbf{S}_{i+1,\alpha} - \frac{1}{4} n_{i,\alpha} n_{i+1,\alpha}) \\ & + J_\perp \sum_{i} (\mathbf{S}_{i,1} \cdot \mathbf{S}_{i,2} - \frac{1}{4} n_{i,1} n_{i,2}) \\ & + t_\parallel \sum_{i,\alpha,\sigma} (\tilde{c}^\dagger_{i,\alpha;\sigma} \tilde{c}_{i+1,\alpha;\sigma} + h.c.) \\ & + t_\perp \sum_{i,\sigma} (\tilde{c}^\dagger_{i,1;\sigma} \tilde{c}_{i,2;\sigma} + h.c.) \,, \end{aligned} \tag{2}$$

where $\tilde{c}^\dagger_{i,\alpha;\sigma} = c_{i,\alpha;-\sigma}(1 - n_{i,\alpha;\sigma})$ are *hole* Guzwiller projected creation operators. The large-U limit of the anisotropic Hubbard ladder leads to antiferromagnetic exchange couplings of the form $J_\beta = 4t_\beta^2/U$ in the two directions $\beta = \parallel, \perp$. Hence, for simplicity, the relation $J_\perp/J_\parallel = (t_\perp/t_\parallel)^2$ will be here assumed even outside of the range $J_\perp/t_\perp \ll 1$ and $J_\parallel/t_\parallel \ll 1$ of rigorous validity of the equivalence between the two models. In the rest of the paper, energies will be measured in units of $t_\parallel$ unless specified otherwise.

2 Single particle spectral function

2.1 Motivations

Let us examine first the one-particle spectral function,

$$A(\mathbf{q},\omega) = A_e(\mathbf{q},\omega) + A_h(\mathbf{q},\omega) \,, \tag{3}$$

where $A_e(\mathbf{q},\omega)$ corresponds to the density of the unoccupied electronic states,

$$A_e(\mathbf{q},\omega) = -\frac{1}{\pi} \mathrm{Im} \big\langle c_{\mathbf{q};\sigma} \frac{1}{\omega + i\epsilon - H + E_0} c^\dagger_{\mathbf{q};\sigma} \big\rangle_0 \,, \tag{4}$$

and $A_h(\mathbf{q},\omega)$ corresponds to the density of the occupied electronic states (*i.e.* unoccupied hole states),

$$A_h(\mathbf{q},\omega) = -\frac{1}{\pi}\mathrm{Im}\big\langle c^\dagger_{\mathbf{q};\sigma}\frac{1}{\omega + i\epsilon + H - E_0}c_{\mathbf{q};\sigma}\big\rangle_0 . \quad (5)$$

Here $\big\langle ...\big\rangle_0$ stands for the expectation value in the ground state wave function of energy E_0. The transverse component of the momentum $\mathbf{q}$ takes only the two values $q_\perp = 0, \pi$ corresponding to symmetric or anti-symmetric states with respect to the reflection exchanging the two chains. $A_h(\mathbf{q},\omega)$ and $A_e(\mathbf{q},\omega)$ are of crucial importance since they can be directly measured in angular-resolved photoemission (ARPES) and inverse photoemission (IPES) spectroscopy experiments, respectively.

Thus far, the role of the anisotropy ratio $t_\perp/t_\parallel$ in dynamical properties of ladders has not been studied in detail, except at half-filling $n = 1$. In this case, the spin gap is remarkably robust and persists down to arbitrary small interchain magnetic coupling $J_\perp$ [23]. The single particle (and two particles) spectral functions of the Hubbard ladder have been obtained at $n = 1$ using quantum Monte-Carlo (QMC) simulations [24]. Working at $U = 8$, two regimes were identified [24] depending on the magnitude of the ratio $t_\perp/t_\parallel$. For instance, increasing $t_\perp$ the half-filled Hubbard ladder evolves from a four-band (at small $t_\perp/t_\parallel$) to a two-band (at large $t_\perp/t_\parallel$) insulator. The latter regime can be understood from the non-interacting $U \sim 0$ picture: in this case, two heavily weighted bonding ($q_\perp = 0$) and anti-bonding ($q_\perp = \pi$) bands are separated by an energy $\sim 2t_\perp$ and the Fermi level lies in between. On the other hand, a small fraction of the total spectral weight is found in the inverse photoemission spectrum ($\omega > \mu$) for $q_\perp = 0$ and in the photoemission spectrum ($\omega < \mu$) for $q_\perp = \pi$. In fact, in the $t_\perp/t_\parallel > 1$ limit, the spin-spin correlation length is very short [24] and a description in terms of a rung Hamiltonian (reviewed in the next section) is appropriate ($t_\parallel$ can then be treated as a small perturbation).

In the other limit $t_\perp/t_\parallel < 1$ of two weakly coupled chains the magnetic correlation length along the chains direction becomes larger. Although no magnetic long range order exists, a description of the single particle properties in terms of a Hartree Fock spin-density-wave (SDW) picture turns out to be reasonably accurate [24]. For both $q_\perp = 0$ and $q_\perp = \pi$ a dispersive structure is observed with a (SDW-like) gap $\sim U$ separating the photoemission and inverse photoemission energy regions. It is worth noticing that the low energy electron or hole excited states now occurs at momentum $\mathbf{q} = \pi/2$ in contrast to the large $t_\perp/t_\parallel$ limit where they occur at momenta $\mathbf{q} = \pi$ ($\omega < \mu$) and $\mathbf{q} = 0$ ($\omega > \mu$). The Hartree-Fock treatment correctly predicts a bandwidth of order $J_\parallel$ due to the magnetic scattering (similar to the spinon-like excitations of the single chain [25]). However, it fails to reproduce the broad incoherent background reminiscent of the holon excitations of the single chain [25].

Away from half-filling ($n = 1$) QMC simulations face the well-known "minus sign" problem (especially at low temperature and large U) which increases the statistical errors and, hence, reduces the accuracy of the analytic continuation to the real frequency axis. Thus far, QMC studies of the doped Hubbard ladder have been restricted to $U \leq 4$ in the range $1.4 \leq t_\perp/t_\parallel \leq 2$ and for temperatures larger than $t_\parallel/8$ [26]. Density matrix renormalization group techniques, on the other hand, can currently only provide information about static correlations [26]. A recently developed variational technique based on the use of a reduced Hilbert space once the ladder problem is expressed in the rung-basis [27] can produce accurate dynamical results on 2×20 clusters at zero temperature and finite hole density [28]. However, this technique has been applied only to isotropic ladders thus far. In the present work, alternative approaches have been used. First, following reference [24], a simple estimation of $A(\mathbf{q},\omega)$ in the single rung approximation has been carried out. This calculation is valid in the limit of small $t_\parallel$ and it is useful in order to discuss the possible existence of metal–insulator transition at commensurate densities such as $n = 0.5$ or $n = 0.75$. This simple analytical scheme gives also a basis for understanding more elaborate numerical calculations. In a second step, exact diagonalization studies based on the Lanczos algorithm were performed to investigate a broad region of parameter space.

2.2 Local rung approximation: metal–insulator transition

Let us consider the limit where $t_\parallel$ is the smallest energy scale, *i.e.* $t_\parallel \ll t_\perp$ and $t_\parallel \ll U$. First, $A(q_\perp,\omega)$ can be calculated straightforwardly at densities $n = 1$ and $n = 0.5$ by diagonalizing exactly the single rung Hamiltonian for 0, 1, 2 and 3 particles (see Ref. [24] for details). At half-filling one obtains,

$$\begin{aligned} A(0,\omega) &= \alpha^2\delta(\omega - \Omega(2,1)) + (1-\alpha^2)\delta(\omega - \Omega(3',2)), \\ A(\pi,\omega) &= (1-\alpha^2)\delta(\omega - \Omega(2,1')) + \alpha^2\delta(\omega - \Omega(3,2)), \end{aligned} \quad (6)$$

where $\alpha^2 = \frac{1}{2}(1 + \frac{1}{\sqrt{U^2+(4t_\perp)^2}})$ and $\Omega(n,m)$ correspond to the excitation energies of the various allowed transitions between a state with m particles to a state with n particles. Here, n, n', n'', *etc.* index the GS and the excited states with n particles on a rung of increasing energy. The poles of the spectral functions are given, also for increasing energies, by

$$\begin{aligned} \Omega(2,1') &= \frac{1}{2}(U - \sqrt{U^2 + (4t_\perp)^2}) - t_\perp , \\ \Omega(2,1) &= \frac{1}{2}(U - \sqrt{U^2 + (4t_\perp)^2}) + t_\perp , \\ \Omega(3,2) &= \frac{1}{2}(U + \sqrt{U^2 + (4t_\perp)^2}) - t_\perp , \\ \Omega(3',2) &= \frac{1}{2}(U + \sqrt{U^2 + (4t_\perp)^2}) + t_\perp . \end{aligned} \quad (7)$$

The chemical potential μ lies between $\Omega(2,1)$ and $\Omega(3,2)$ leading to the same integrated spectral weight ($= 1$) in the photoemission and inverse photoemission parts of the spectrum for all values of U. Hence, as expected,

the system is an insulator with a single particle gap of $\Delta_{eh} = \sqrt{U^2 + 16t_\perp^2} - 2t_\perp$. However, since the weight α^2 varies strongly with the ratio $U/4t_\perp$, the distribution of spectral weight changes qualitatively for increasing U as shown in Figures 1a, 1b. At small U, $\alpha^2 \sim 1 - \frac{1}{4}(\frac{U}{4t_\perp})^2$ and one recovers, as in the non-interacting limit, two highly weighted bonding (at an energy around $-t_\perp$) and antibonding (at an energy around $t_\perp$) bands. When $U \to \infty$, $\alpha^2 \to 1/2$ and, thus, with increasing U spectral weight is transferred to bonding and antibonding states further away from the chemical potential. In the large $U/4t_\perp$ regime, the system becomes a four-band insulator with 4 (almost) equally weighted poles and a Hubbard gap of order U separating bonding or anti-bonding states at $\omega < \mu$ and $\omega > \mu$.

Note that a similar transition from a two-band to a four-band insulator has also been observed in QMC studies of the half-filled Hubbard ladder [24] at finite $t_\parallel$ and fixed value $U/t_\parallel = 8$ by decreasing the ratio $t_\perp/t_\parallel$ from 2 to 0.5. In fact, $U/t_\parallel = 8$ and $t_\perp/t_\parallel = 2$ correspond to the intermediate regime $U/4t_\perp = 1$ where, according to the previous $t_\parallel \to 0$ estimate, only $\sim 15\%$ of the spectral weight is located in the side bands. For smaller $t_\perp$, more weight appears at the position of these two additional structures leading to four bands. In general, for arbitrary ratio $t_\perp/t_\parallel$, one expects a transition to a four-band insulator when U becomes sufficiently large compared to the *largest* of the two hopping matrix elements *i.e.* $U \gg \max\{t_\perp, t_\parallel\}$.

Let us now turn to the discussion of the quarter-filled case $n = 0.5$ where a similar local rung calculation leads to,

$$\begin{aligned} A(0,\omega) &= \frac{1}{2}\,\delta(\omega - \Omega(1,0)) + \frac{1}{2}\alpha^2\,\delta(\omega - \Omega(2,1)) \\ &\quad + \frac{1}{2}(1-\alpha^2)\,\delta(\omega - \Omega(2''',1))\,, \qquad (8) \\ A(\pi,\omega) &= \frac{3}{4}\,\delta(\omega - \Omega(2',1)) + \frac{1}{4}\,\delta(\omega - \Omega(2'',1))\,, \end{aligned}$$

where the new energy poles are given by

$$\begin{aligned} \Omega(1,0) &= -t_\perp\,, \\ \Omega(2',1) &= t_\perp\,, \qquad (9) \\ \Omega(2'',1) &= t_\perp + U\,, \\ \Omega(2''',1) &= \Omega(3',2)\,. \end{aligned}$$

Since the chemical potential is located exactly *between* $\Omega(1,0)$ and $\Omega(2',1)$, the system is an insulator for all values of U and (sufficiently) small $t_\parallel$ (compared to U). However, $A(q_\perp,\omega)$ exhibits completely different forms at small and large U couplings as observed in Figures 1c, 1d. At small U, as in the non-interacting case, the bonding states and antibonding states are separated by an energy of order $2t_\perp$. However, each structure is split by a small energy proportional to U and the chemical potential lies between the two $q_\perp = 0$ sub-bands. For large U, the gap becomes of order $2t_\perp$ and upper Hubbard bands (of almost equal weights) of the bonding and anti-bonding states appear at an energy $\sim U$ higher. Although this picture does not take into account $t_\parallel$, the role of a small $t_\parallel$ can be easily discussed qualitatively. In fact $t_\parallel$ is expected to give a dispersion in the chain direction and a width to the various structures discussed here. When $4t_\parallel$ becomes comparable to the single particle excitation gap Δ_{eh}, bands will start to overlap and a transition from the insulator to a metallic state is expected [29], as will be discussed in the next section. Since the single particle excitation gap $\Delta_{eh} = \frac{1}{2}(U - \sqrt{U^2 + 16t_\perp^2}) + 2t_\perp$ is of the order of the smallest of the two energy scales $U/2$ and $2t_\perp$, the insulating phase is then restricted to the range $4t_\parallel < \min\{U/2, 2t_\perp\}$.

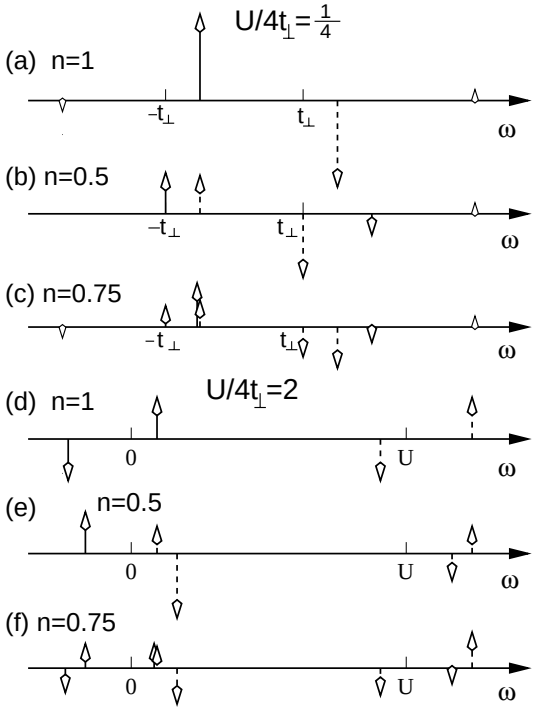

Fig. 1. Schematic representation of the single particle spectral function *vs.* frequency, in the $t_\parallel \to 0$ limit. The position of the single particle energy poles are indicated by arrows whose lengths are proportional to the spectral weights associated to the corresponding transitions. Arrows pointing upwards (downwards) correspond to $q_\perp = 0$ ($q_\perp = \pi$). The photoemission peaks (occupied states) and the inverse photoemission peaks (empty states) correspond to full line and dashed line arrows, respectively. The spectra are shown for ratios $\frac{U}{4t_\perp} \simeq 1/4$ ((a), (b) and (c)) and $\frac{U}{4t_\perp} \simeq 2$ ((d), (e) and (f)) and for electron densities $n = 1$, $n = 0.5$ and $n = 0.75$ as indicated.

The existence of a metal-insulator transition is, in fact, specific to quarter filling (besides the half-filled case which is always insulating). A simple argument is here presented to show that at other (commensurate) densities such as $n = 0.75$ the metallic phase (*i.e.* with at least one gapless charge mode) is stable for arbitrary small $t_\parallel$. At $n = 0.75$, a local rung calculation of $A(q_\perp,\omega)$ requires to consider as a GS two decoupled rungs on 4 sites with 2 and 1 particle, respectively. The spectral function is then given

straightforwardly by the average of the spectral function equations (6, 8) at densities $n = 1$ and $n = 0.5$. However, the location of the chemical potential is a subtle issue: since the states at the energy $\omega = \Omega(2,1)$ are completely filled (empty) for $n = 1$ ($n = 0.5$), it is clear that this state will become *partially* filled at $n = 0.75$ so that the chemical potential is pinned at this energy. Consideration of the spectral weights of the excitations shows immediately that, for arbitrary small $t_\parallel$, the band centered at $\omega = \Omega(2,1)$ (of weight $\frac{3}{4}\alpha^2$) is always $\frac{2}{3}$–filled leading to a metallic behavior. In this case, an additional interaction, *e.g.* between nearest neighbor sites along the chains, would be required to produce a metal-insulator transition. Schematic representations of $A(q_\perp, \omega)$ at $n = 0.75$ are shown in Figures 1c, 1f at small and large U. At small U, as expected, the two bonding and anti-bonding structures separated by $\sim 2t_\perp$ are clearly visible and the bonding states at the lower energies are partially occupied. In this limit, U leads essentially to small splittings of the various structures into sub-bands (as for $n = 0.5$). For large U, the spectral function is qualitatively very different with 2 distinct bands around $-t_\perp$ and $t_\perp$ for both $q_\perp = 0$ and $q_\perp = \pi$ states. However, the upper Hubbard band around an energy $\sim U$ is formed of two peaks (separated by $2t_\perp$) for $q_\perp = \pi$ while only one peak is present for $q_\perp = 0$.

Finally in this section a brief discussion of the case of the $t - J$ ladder is included. Since this model describes only the low energy properties of the Hubbard model, the corresponding spectral functions in the $t_\parallel \to 0$ limit can be obtained easily from the previous ones by discarding the high energy peaks whose energy scales as U for large–U, setting $\alpha^2 = 1/2$ and expanding energies to first order in $J_\perp = 4t_\perp^2/U$. In fact, it can be easily shown that the same expressions hold for the $t - J$ model (with arbitrary $J_\perp$). Note that, due to the projection of the high energy states, the spectral function of the $t - J$ model follows the new sum-rule $\int A(q_\perp, \omega)\, d\omega = \frac{1+x}{2}$ (instead of 1), where $x = 1 - n$ is the doping fraction. At half-filling one gets:

$$A(0,\omega) = \frac{1}{2}\,\delta(\omega - (t_\perp - J_\perp))\,,$$
$$A(\pi,\omega) = \frac{1}{2}\,\delta(\omega - (-t_\perp - J_\perp))\,, \qquad (10)$$

with the chemical potential located at an higher energy ($\sim U/2$). Similarly, at quarter-filling one obtains,

$$A(0,\omega) = \frac{1}{2}\,\delta(\omega - (-t_\perp)) + \frac{1}{4}\,\delta(\omega - (t_\perp - J_\perp))\,,$$
$$A(\pi,\omega) = \frac{3}{4}\,\delta(\omega - t_\perp)\,, \qquad (11)$$

with the chemical potential located between $-t_\perp$ and $t_\perp - J_\perp$. It is interesting to notice that, when $J_\perp$ exceeds $2t_\perp$, the electron-like excitation becomes lower in energy than the hole-like excitation. This signals the onset of phase separation or, alternatively, some sort of charge localization/ordering (such as charge density wave ordering). Physically, this occurs when the magnetic energy gain of a singlet on a single rung becomes larger than the kinetic energy of two particles on individual rungs.

2.3 Exact diagonalization results: Hubbard model

Let us now investigate the dynamical properties of the Hubbard and $t - J$ models for arbitrary parameters using exact diagonalization techniques. Cyclic $2 \times L$ ladders are diagonalized and the (zero temperature) particle spectral function is obtained exactly by a standard continued-fraction procedure. Although in practice one is limited to $L = 8$ (for the Hubbard model), both periodic (PBC) and anti-periodic (ABC) boundary conditions can be used to consider a sufficiently large number of momenta $q_\parallel = n\frac{\pi}{L}$, $n = 0, 2L - 1$.

The case of the Hubbard ladder will be considered first, before focusing on the low energy excitations described by the $t-J$ model. The spectral function $A(\mathbf{q}, \omega)$ at a density of $n = 0.75$ is shown in Figure 2 for $U = 8$ and several values of $t_\perp$ ranging from 2.5 down to 0.5. Note that both PBC and ABC have been used in Figure 2b while, in order to reduce CPU time, only ABC (PBC) have been used in Figure 2a (Fig. 2c). Two sharp structures separated by an energy proportional to $t_\perp$ can be attributed to a bonding and an anti-bonding band. At the largest ratio of $t_\perp/t_\parallel = 2.5$ that have been considered, the spectrum exhibits some features of Figure 1c obtained in the local rung approximation at small coupling: (i) in the photoemission part, a $q_\perp = 0$ sub-band of small spectral weight can be observed at an energy of about $U/2$ from the main $q_\perp = 0$ band crossing the chemical potential; (ii) a $q_\perp = \pi$ upper Hubbard band appears at an energy $\propto U$ away from the main (empty) $q_\perp = \pi$ band. On the other hand, some tiny structures characteristic of the strong coupling limit (Fig. 1f) can also be observed: (i) a small spectral weight exists at $\omega < \mu$ (around $\omega \sim -5$) for $q_\perp = \pi$ together with (ii) a quite small $q_\perp = 0$ upper Hubbard band at $\omega > \mu$. Interestingly enough, these features become more important for $t_\perp = 1.5$ as shown in Figure 2b which corresponds, in fact, to a larger ratio $U/4t_\perp \simeq 1.3$.

With decreasing electron density, the respective position of the two main bands and the position of the Fermi level seems to evolve as in a rigid-band scheme. However, there are important differences: (i) the bandwidth is strongly reduced specially at smaller $t_\perp/t_\parallel$; (ii) the excitations become sharper when the band crosses the chemical potential. To the best of our knowledge, this is the first observation in a numerical study of the broadening of the "quasi-particle"-like peaks excitations as one moves away from the chemical potential.

For a larger hole doping and working at a commensurate value of $n = 0.5$ qualitative changes can take place in the spectral function at sufficiently large U and $t_\perp$. Data are shown in Figure 3. For $t_\perp = 0.5$ the two partially filled bonding and antibonding bands can be observed together with their corresponding upper Hubbard bands at higher energy. As expected from the previous $t_\parallel \to 0$ analysis, the spectral weight of the $q_\perp = 0$ upper Hubbard band, at fixed U, gets strongly reduced for increasing $t_\perp$ *i.e.* for a decreasing ratio $U/t_\perp$. At large enough $t_\perp$, a gap appears in the $q_\perp = 0$ structure, leading to two sub-bands and an insulating behavior in agreement with the local rung calculation. Such a metal-insulator transition is induced

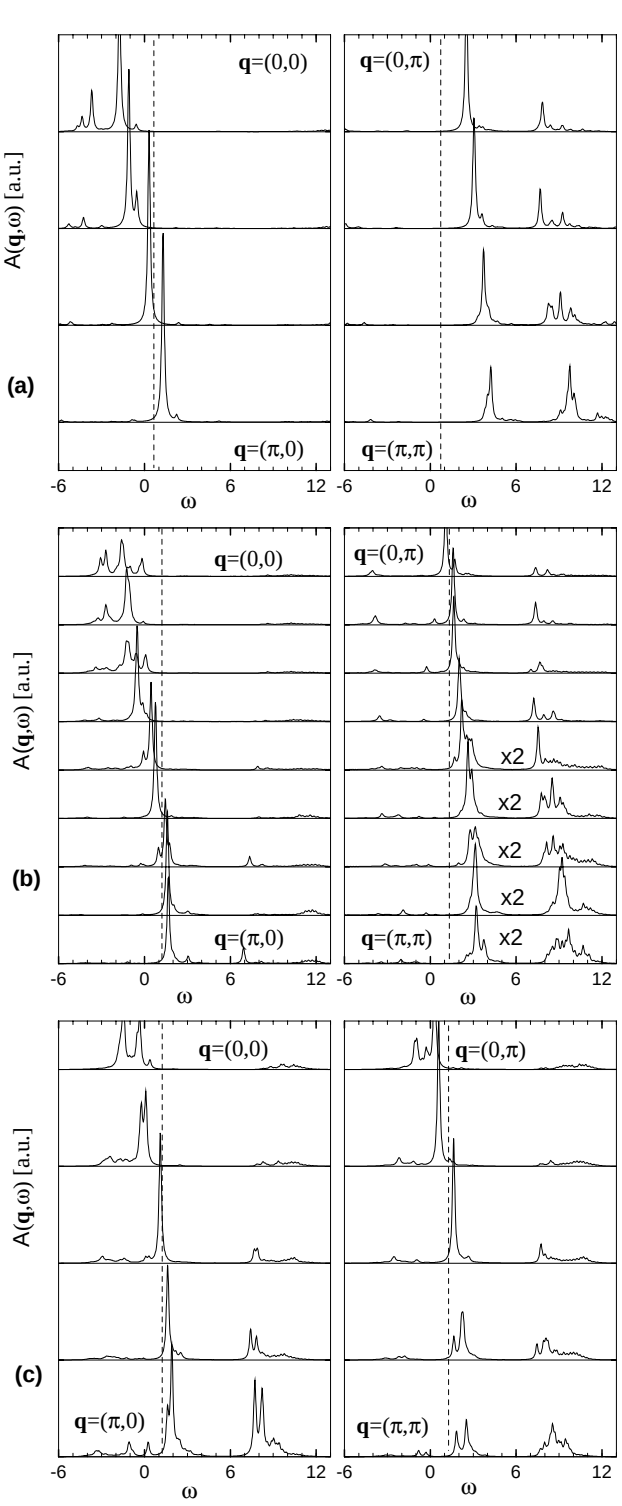

Fig. 2. Spectral function $A(\mathbf{q},\omega)$ of the Hubbard ladder for $U = 8$ and $n = 0.75$. The left and right sides correspond to the bonding ($k_y = 0$) and anti-bonding states ($k_y = \pi$), respectively, and k_x runs from 0 to π from the top to the bottom. The position of the chemical potential is indicated by a vertical dotted line. (a), (b) and (c) correspond to $t_\perp = 2.5$, $t_\perp = 1.5$ and $t_\perp = 0.5$, respectively.

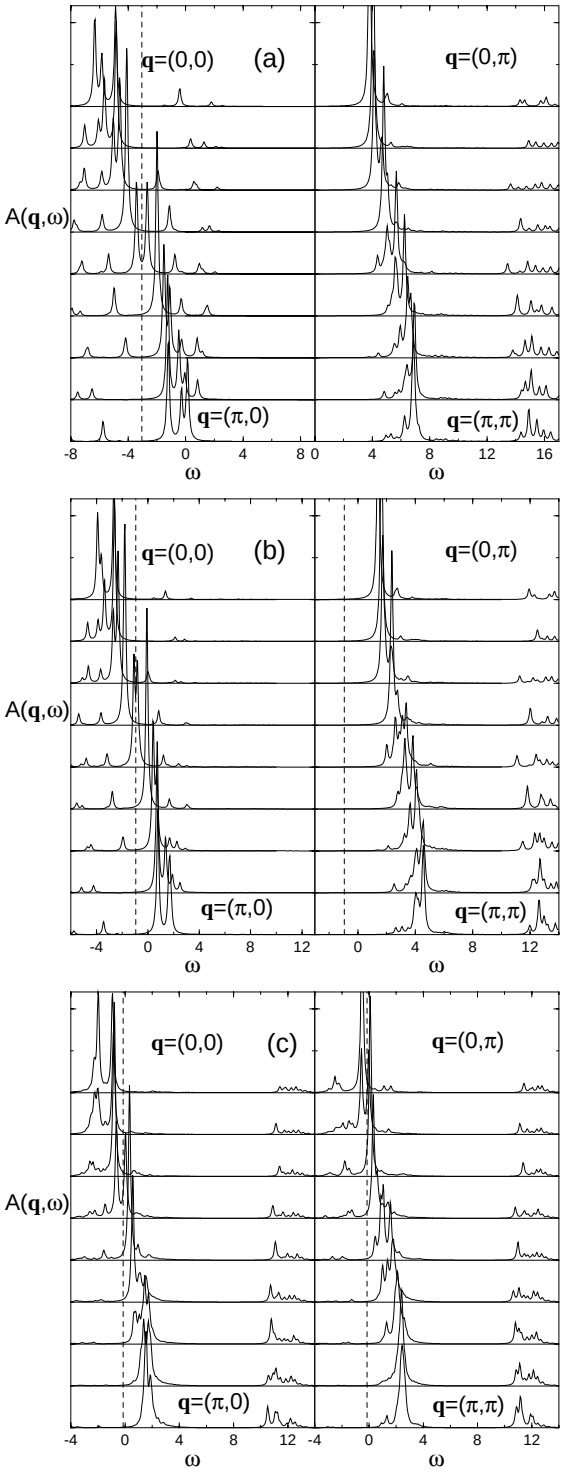

Fig. 3. Spectral function $A(\mathbf{q},\omega)$ of the Hubbard ladder for $U = 10$ at quarter-filling $n = 0.5$. The left and right sides correspond to the bonding ($k_y = 0$) and anti-bonding states ($k_y = \pi$), respectively, and k_x runs from 0 to π from the top to the bottom. (a), (b) and (c) correspond to $U = 10$ with $t_\perp = 5$, $t_\perp = 2.5$ and $t_\perp = 0.5$ respectively.

by a combined effect of $t_\perp$ and U: when $t_\perp$ is large enough the lower band becomes half-filled and a finite U, leading to relevant Umklapp scattering, can then open a gap.

2.4 Exact diagonalization results: t − J model

In order to study more precisely the influence of doping at small energy scales let us now focus on the $t-J$ ladder [30]. Results at small hole densities $n = 0.875$ and $n = 0.75$ are shown in Figures 4 and 5 and are consistent with the previous results on the Hubbard model.

Let us first discuss the role of the hole doping $x = 1-n$, for the largest value of $t_\perp = 2$ considered here (see Fig. 4a and Fig. 5a). For this choice of parameters, the x-dependence can be qualitatively understood from the single rung picture. For $t_\parallel \to 0$ the GS contains a density of $2x$ singly occupied bonds and $1-2x$ doubly occupied bonds. By combining the spectral functions at $n = 0.5$ and $n = 1$ with the respective weights, one obtains a simple picture of the influence of doping consistent with the numerical results at small (but finite) $t_\parallel$. The $q_\perp = 0$ main structure (which is the closest to the chemical potential at half-filling) becomes partially filled with a weight of $x/2$ in the inverse photoemission part $\omega > \mu$. Note that the dispersion of the band is especially flat in the vicinity of the chemical potential at small x. With increasing doping, weight is transferred from this structure (of total weight $1/2 - x/2$) and from the upper Hubbard band (not described by the $t-J$ model) to $q_\perp = 0$ states further away from the chemical potential. This leads to an emerging structure of weight x at an energy of $\sim 2t_\perp - J_\perp$ below the main band. Physically, in a photoemission experiment, these small peaks correspond to processes where an electron on a singly occupied rung is removed by a photon and leaves behind an empty rung. Note that this structure becomes particularly strong at quarter filling (as seen in Fig. 6a) where it carries $1/2$ of the total spectral weight (normalized to 1). In the $q_\perp = \pi$ sector, the main structure in the photoemission part of the spectrum $\omega < \mu$ (barely seen in the case of the Hubbard model for the parameters chosen in the previous study) is also loosing spectral weight upon doping with a total weight of $1/2 - x$. The missing weight (and some additional spectral weight from the upper Hubbard band) is transferred into the inverse photoemission spectrum leading to an emerging band of total weight $3x/2$ at $\omega > \mu$. Such states, obtained by suddenly adding an electron on a singly occupied rung could be seen in an inverse photoemission experiment. At quarter filling $n = 0.5$, as seen in Figure 6a, the transfer of spectral weight is complete and the $\omega < \mu$, $q_\perp = \pi$ structure has totally disappeared.

At smaller values of $t_\perp$ (see Figs. 4b, 4c, 5b and 5c) the two separate structures, both for $q_\perp = 0$ or $q_\perp = \pi$, merge into a single broad structure. The data can be fairly well described by (i) $q_\perp = 0$ and $q_\perp = \pi$ bands dispersing through the chemical potential and (ii) a broad incoherent background extending further away from the chemical potential towards negative energies. Note that, similarly to the previous case of the Hubbard model,

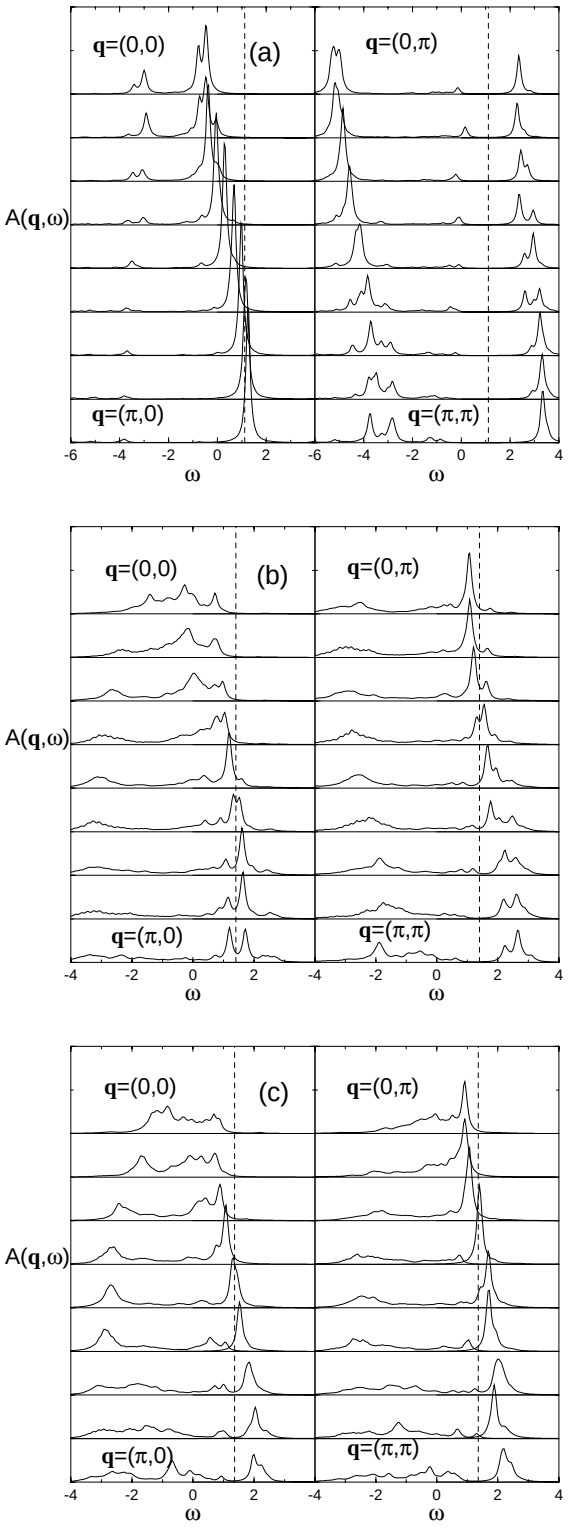

Fig. 4. Spectral function $A(\mathbf{q},\omega)$ of the $t-J$ ladder at $n = 0.875$ and $J_\parallel = 0.4$. Conventions are similar to those of Figure 2. (a), (b) and (c) correspond to $t_\perp = 2$, $t_\perp = 1$ and $t_\perp = 0.5$, respectively.

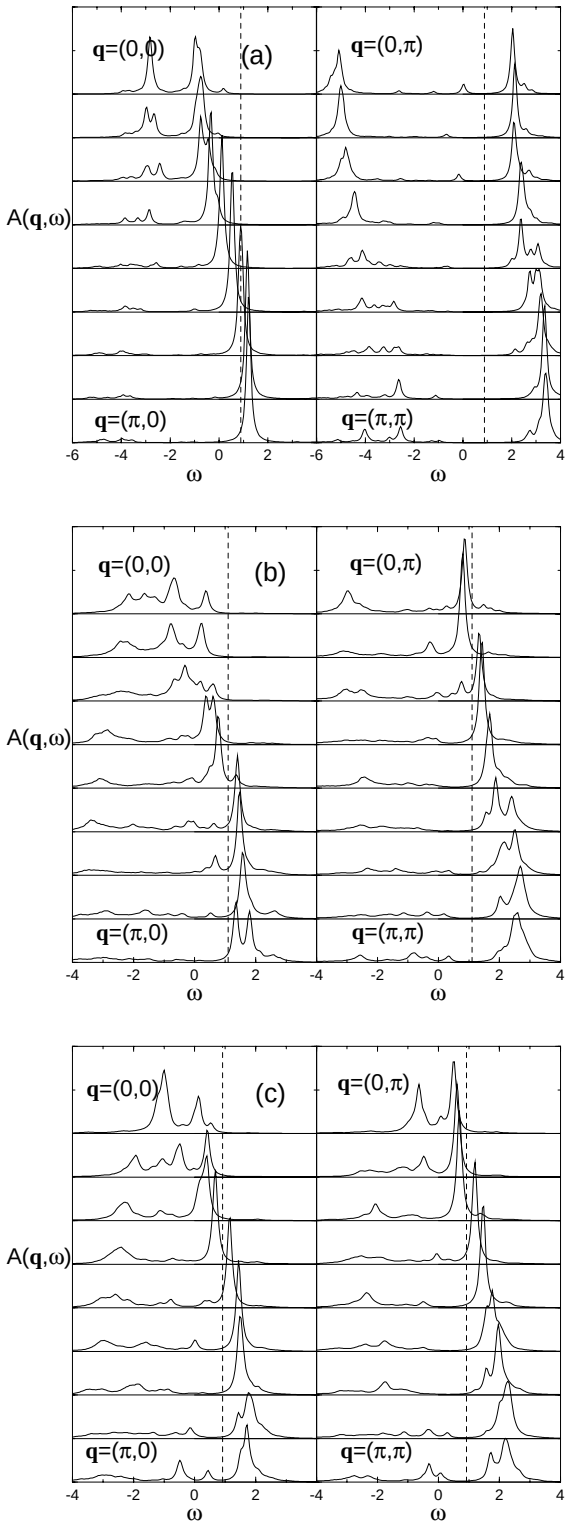

Fig. 5. Spectral function $A(\mathbf{q},\omega)$ of the $t-J$ ladder at $n = 0.75$ and $J_\parallel = 0.4$. Conventions are similar to those of Figure 2. (a), (b) and (c) correspond to $t_\perp = 2$, $t_\perp = 1$ and $t_\perp = 0.5$, respectively.

the peaks of the band-like feature seem to become narrower when they cross the chemical potential as expected in a Fermi liquid description.

This section ends with a short discussion on the possible existence of small single particle gaps in the previous data. The quarter-filled case is qualitatively different from the low doping regime. At $n = 0.5$ the $t_\parallel \to 0$ analysis unambiguously predicts the existence of a gap in the single particle spectrum at sufficiently large $t_\perp$ and U. However, when the $q_\perp = \pi$ structure is not completely empty (*i.e.* totally located in the $\omega > \mu$ region of the spectrum), as it is the case in Figures 3c, 6b and 6c, no gap is expected as it is clear in the numerical data. Then, a metal–insulator transition is expected by increasing $t_\perp$ but whether this transition is driven by $t_\perp$ alone is still unclear. The data of Figures 3a, 3b corresponding to a situation where the antibonding band is clearly unoccupied do not allow to accurately determine a critical value of $t_\perp$ at which the gap starts to grow. However, we have checked numerically (not shown) that, by reducing $t_\parallel$, the spectrum of Figure 3a smoothly evolves into the spectrum obtained above in the single rung approximation, *e.g.* exhibiting a well defined gap at the chemical potential.

At small doping, on the other hand, the physical origin of a small single particle gap would be quite different. In this case, it would be related to the formation of pairs. In the $t_\parallel \to 0$ limit, pairs become stable only when $J_\perp > 2t_\perp$, *i.e.* when the magnetic energy on a rung exceeds the kinetic energy loss. Otherwise, for $J_\perp < 2t_\perp$, the spin gap is immediately destroyed by doping (strictly for $t_\parallel = 0$) since the presence of singly occupied rungs leads to new low-energy spin-1 excitations in the $n = 1$ spin gap (of order $J_\perp$). Therefore, intermediate ratios of $t_\perp/t_\parallel$ seem to be more favorable for pair binding. Although spectra like those shown in Figures 4b, 5b are not inconsistent with the presence of a small gap at the chemical potential, the study of pair binding from an investigation of the spectral function at small energy scales around the chemical potential is a difficult task. In order to clarify this issue, a complementary study of static physical quantities is shown in the next section.

3 Superconducting properties

3.1 Pair binding energy

In the limit where $J_\perp$ is the largest energy scale, formation of hole pairs are favored on the rungs in order to minimize the magnetic energy cost. In fact, this simple naive argument breaks down when $t_\perp > J_\perp/2$ since holes on separate rungs can then benefit from a delocalization on each rung. In the large $t_\perp$ limit, a simple 4-sites (2 rungs) calculation shows that for $J_\perp/2 << t_\perp$, the pair binding energy (which, as defined below, should be positive if a bound state exists) behaves as $J_\parallel^2/4t_\perp - 2t_\parallel$. Very tightly bound hole pairs are then not stable in the intermediate regime. However, extended pairs have been shown to exist in some regime [6,9,31]. In this section, the stability

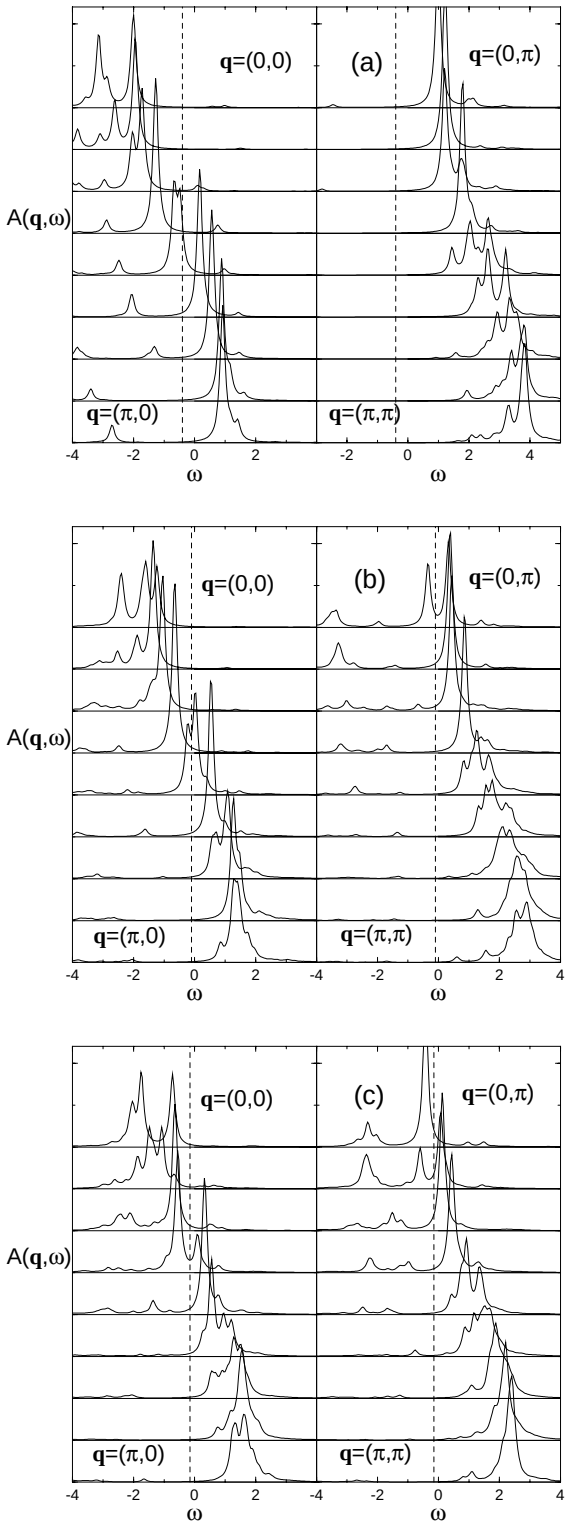

Fig. 6. Spectral function $A(\mathbf{q},\omega)$ of the $t-J$ ladder at $n=0.5$ and $J_\parallel = 0.2$. Conventions are similar to those of Figure 2. (a), (b) and (c) correspond to $t_\perp = 2$, $t_\perp = 1$ and $t_\perp = 0.5$, respectively.

of the hole pairs as a function of the anisotropy ratio will be investigated in detail.

To study the onset of pair binding, irrespective of the actual size of the pair, the two-hole binding energy defined by

$$\Delta_B(L) = 2E(L,1) - E(L,2) - E(L,0)\,, \qquad (12)$$

is considered, with $E(L,N_h)$ being the GS energy of the $2\times L$ ladder doped with N_h holes. $E(L,N_h)$ ($N_h = 0,1,2$) have been calculated on $t-J$ ladders with periodic or anti-periodic boundary conditions along the legs direction and considering sizes up to $L=13$. As previously, it has been assumed for convenience that $J_\perp = J_\parallel (t_\perp/t_\parallel)^2$. Typical finite size behaviors of $\Delta_B(L)$ are shown in Figure 7 for different anisotropy ratios. Some caution is obviously needed in order to extrapolate the results to the thermodynamic limit. At large $t_\perp$ for a fixed choice of the boundary conditions very regular oscillations in Δ_B *vs.* L appear (as observed for instance in Fig. 7a). However, the data set corresponding to ladders with an even (odd) number of rungs (L) and PBC can be combined with the data set corresponding to ladders with an odd (even) number of rungs and ABC. The two resulting curves exhibit a smooth behavior (full lines) which allow an accurate extrapolation to the thermodynamic limit. For intermediate values of $t_\perp/t \sim 1.25$, the two data sets merge into a single curve and finite size corrections become particularly small.

For smaller ratios such as $t_\perp/t_\parallel \leq 1$ (see Fig. 7b), there is a qualitative change of behavior. In this case, the data corresponding to ladders with an *odd* number of rungs ($L=2p+1$) have to be distinguished from the data obtained for $L=2p$. Indeed, in this parameter regime, the spin correlation length along the chains becomes of the order of the system size so that ladders with $L=2p$ and 2 holes suffer from a small magnetic frustration induced by the boundary conditions. An accurate finite size scaling analysis can nevertheless be realized by considering the data for $L=2p+1$ which show again a very systematic behavior as a function of L; in fact, although the behavior of the data sets corresponding to ladders with $L=4p+1$ ($L=4p+3$) rungs and PBC follow only roughly the same trend as the data set corresponding to ladders with $L=4p+3$ ($L=4p+1$) rungs and ABC, averaging over PBC and ABC leads to a single remarkably smooth behavior of Δ_B *versus* L as observed in Figure 7b. A similar procedure can be followed for the data obtained with $L=2p$ as shown also in Figure 7b but this extrapolation is probably less reliable for the reasons stated above. In all cases, the $L\to\infty$ extrapolation is performed according to $\Delta_B(L) = \Delta_B^\infty + A\frac{1}{L}\exp(-L/\xi)$, where Δ_B^∞, ξ and A are free parameters determined from a fit to the data.

The extrapolated values of Δ_B are displayed in Figure 8 as a function of $t_\perp$ for $J_\parallel = 0.5$. A positive binding energy (implying the stability of the hole pair) is obtained for all parameters considered here. Recent DMRG work using clusters with up to 2×30 sites and two holes have calculated the binding energy

in the isotropic limit [32]. The result $\Delta_B \sim 0.2$ reported there is very close to the number found by our size extrapolation in Figure 8, giving extra support to our procedure. For comparison, the spin gaps Δ_0 and Δ_2 in the undoped GS and 2 hole doped GS, respectively are also shown. The scaling behavior of Δ_2 is very similar to that of Δ_B as can be seen in Figures 7c, 7d (although finite size effects are larger) and the same procedures to obtain the extrapolations to $L = \infty$ have been used. Our extrapolations for Δ_0 are in good agreement with previous ED [33] and QMC [34] estimates or with the weak coupling limit behavior $\Delta_0 \sim 0.41 J_\perp$. The behaviors of Δ_B and Δ_2 with $t_\perp$ are very similar, and both have a pronounced maximum of Δ_B at $t_\perp/t \sim 1.25$. In fact it is expected that in the 2 hole doped GS the lowest $S = 1$ excitations can be obtained by either (i) breaking up a hole pair and flipping one of the unpaired spins or (ii) making a spin excitation away from the hole pair (which is supposed to have a finite size). Therefore, one expects $\Delta_2 = \min\{\Delta_B, \Delta_0\}$. Our data indeed suggest two regimes: (i) For $t_\perp/t_\parallel \leq 1.25$, the binding energy of a pair is larger than the spin gap in the undoped system. This extra stability of the hole pair is probably due to the strong antiferromagnetic correlations within each chain. Note that, in this regime, there are some small discrepancies between Δ_2 and Δ_0. This effect is probably due to the fact that the size of the pair is particularly large for such parameters and the two regions corresponding to the undoped spin liquid and the hole pair cannot truly separate in the clusters that can be handled computationally leading to strong finite size effects for Δ_2. (ii) For $t_\perp/t_\parallel \geq 1.25$, the hole binding energy strongly decreases and the lowest spin excitation is obtained by breaking a hole pair *i.e.* $\Delta_2 \sim \Delta_B$. Note that for even larger ratios $t_\perp/t_\parallel$ (typically $t_\perp/t_\parallel > 2.5$), the binding energy increases again. Clearly, this is an artificial effect due to the fact that, in our model, the rung magnetic coupling scales like $t_\perp^2$ and becomes unphysically large compared to $t_\perp$ for large enough $t_\perp$. In that case, $\Delta_B \simeq J_\perp - 2t_\perp$ which approaches the spin gap Δ_0 for large $t_\perp$.

It is interesting to compare the results of Figure 8 with the previous study of the collective modes of the $t-J$ ladder [11]. On general grounds, two collective spin modes of momenta $q_\perp = 0$ and $q_\perp = \pi$ are expected in a doped spin ladder. Both modes are gapped at moderate doping [11]. From a careful examination of the quantum numbers of the various spin excitations shown in Figure 8, one can safely study, at vanishing doping (*i.e.* for 2 holes in an infinitely large system), each low energy excitation. The collective $q_\perp = \pi$ spin mode corresponds to the spin excitation of energy Δ_0 characteristic of the undoped system (crudely an excitation of a singlet rung into a triplet). On the other hand, the $q_\perp = 0$ spin mode is associated to the breaking of a hole pair of energy Δ_B. From our previous analysis of the data, a level crossing occurs between these two types of excitations around $t_\perp \simeq 1.25$ producing a cusp-like maximum of Δ_2.

Materials corresponding to the regime $t_\perp/t_\parallel > 1.25$ should be particularly interesting to be studied by

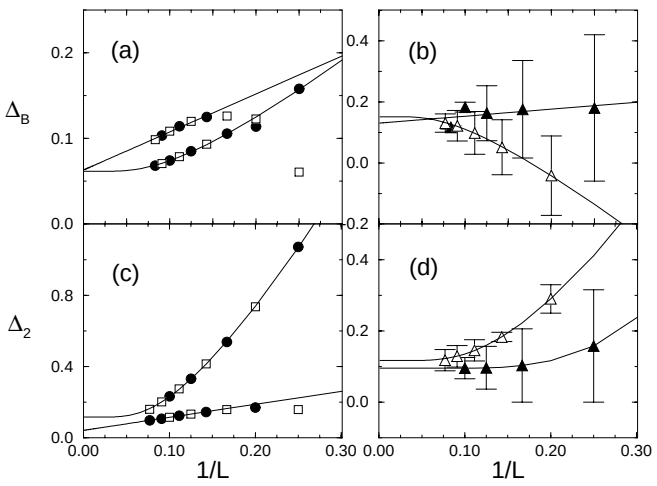

Fig. 7. Finite size scaling behaviors as a function of the inverse of the ladder length for $J_\parallel = 0.5$. Filled circles (open squares) correspond to PBC (ABC). The values of $t_\perp$ are shown on the plot. The full lines correspond to the finite size scaling laws used for the extrapolations to $L = \infty$. (a) Two hole binding energy for $t_\perp = 2.25$; (b) Two hole binding energy for $t_\perp = 1/\sqrt{2}$; (c) Finite size behavior of the triplet gap in the GS with 2 holes for $t_\perp = 2.25$; (d) Finite size behavior of the triplet gap in the GS with 2 holes for $t_\perp = 1/\sqrt{2}$; In (b) and (d), the triangles correspond to averages between the PBC and the ABC data and the sizes of the error bars correspond to the absolute value of the difference between the two sets. Open (filled) symbols correspond here to L odd (even).

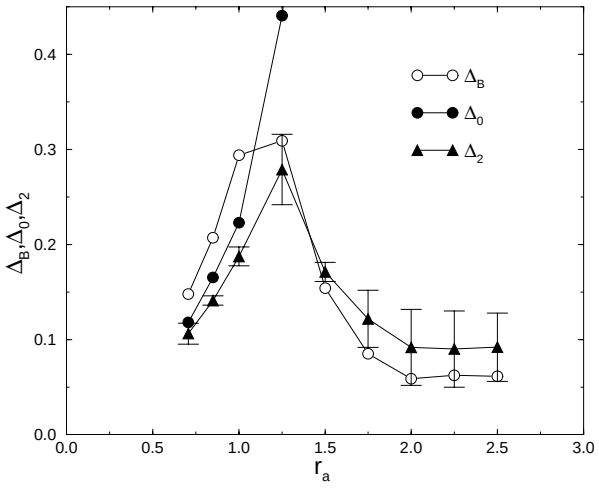

Fig. 8. Extrapolated two hole binding energy (open symbols) as a function of the anisotropy $r_a = t_\perp/t_\parallel$ for $J_\parallel = 0.5$. Spin gaps in the half-filled and two hole doped GS are also shown for comparison (filled symbols).

Inelastic Neutron Scattering (INS) experiments at small doping. Indeed, the above calculation predicts that, under light doping, spectral weight in the dynamical spin structure factor $S(\mathbf{q},\omega)$ should appear *within* the spin gap of the undoped material. This new $q_\perp = 0$ magnetic structure whose total weight should roughly scale with the doping fraction corresponds to the excitations of hole pairs into two separate holes in a triplet state. The corresponding energy scale for such excitations can be much lower than the spin gap of the undoped spin liquid GS ($q_\perp = \pi$).

The maximum observed in Δ_B for the $t-J$ model at $J_\parallel = 0.5$ as a function of $t_\perp$ has similarities with the behavior of the pair-pair correlation obtained in the Hubbard model at very small hole doping [26] $n = 0.9375$ which also shows a maximum (around $t_\perp \simeq 1.4$ for $U = 8$). In reference [26], this particular value of $t_\perp$ was associated with the situation where the chemical potential coincides almost exactly with the top of the lower bonding band and with the bottom of the upper antibonding band. In that case, one expect a particularly large density of state at the chemical potential (see also Ref. [38]). However, such a correspondence was made possible at smaller U only (due to difficulties to obtain accurate QMC calculations of dynamical quantities at intermediate and large values of U). The spectral function $A(\mathbf{q},\omega)$ shown in Figure 4b was obtained in the two hole GS of the 2×8 ladder for a choice of parameters ($J_\parallel = 0.4$ and $t_\perp = 1$) close to the ones producing the maximum of Δ_B in Figure 8. Figure 4b clearly shows a large density of states in the vicinity of the chemical potential due to the flatness of the dispersion around $\mathbf{q} = (0,\pi)$ or $\mathbf{q} = (\pi,0)$. This situation corresponds to the cross-over between the two band and four band insulator regimes observed at half-filling [24]. It is also interesting to note that a small depression of the density of state is visible in Figure 4b at the chemical potential. This could be interpreted as a small gap associated to the existence of a bound pair. More generally, in the so called $C1S0$ phase [13,15,18] where the spin gap survives, one expects to see its signature in $A(\mathbf{q},\omega)$ as a gap at the chemical potential. However, the energy scale of the spin gap is small (see *e.g.* the order of magnitude of Δ_2 in Fig. 8) compared to the various features that appear in $A(\mathbf{q},\omega)$ and thus, in most cases, its manifestation in $A(\mathbf{q},\omega)$ cannot be observed on small lattices. In the recent studies using a reduced Hilbert space, a gap caused by pairing in the spectral function was observed on clusters with 2×16 and 2×20 sites [28] in agreement with the data of Figure 4b.

3.2 Pair-pair correlations

ED studies supplemented by conformal invariance arguments suggest that in the doped spin gap phase ($C1S0$) of the isotropic $t-J$ ladder (where pairs are formed according to the previous analysis) algebraic superconducting and $4k_F$-CDW correlations are competing [15]. At small J/t ratio, the CDW correlations dominate while above a moderate critical value of J/t coherent hopping of the pairs takes over. The aim of the present section is to investigate the role of the anisotropy $t_\perp/t_\parallel$ by a direct calculation of the pair-pair correlation as a function of distance. As previously, in the case of the $t-J$ model, a rung magnetic coupling $J_\perp = J_\parallel (t_\perp/t_\parallel)^2$ is used.

Superconducting correlations can be evidenced from a study of the long distance behavior of the pair hopping correlation,

$$C_S(r-r') = \left\langle \Delta^\dagger(r)\Delta(r')\right\rangle_0 , \tag{13}$$

where $\Delta^\dagger(r)$ is a creation operator of a pair centered at position labeled by r. Although the best choice of $\Delta^\dagger(r)$ clearly depends on the internal structure of the hole pair [35] as discussed later, it should exhibit general symmetry properties associated to the quantum numbers of the hole pair found in the previous section: (i) $\Delta^\dagger(r)$ is a singlet operator and (ii) it is even with respect to the two reflection symmetries along and perpendicular to the ladder direction (and centered at position r). The static correlation function of equation (13) can be interpreted as a coherent hopping of a pair centered at position r to a new position r'.

According to conformal invariance, in a strictly 1D ladder (which is the case studied here) the pair hopping correlation exhibits a power-law behavior at large distances $|r-r'|$,

$$C_S(r-r') \sim 1/|r-r'|^{\frac{1}{2K_\rho}} , \tag{14}$$

where the exponent K_ρ was calculated in the weak coupling limit [13] or in the isotropic $t-J$ ladder by ED methods using conformal invariance relations [15]. Superconducting correlations dominate when $K_\rho > 1/2$ which occurs for $J/t > 0.3$ in the lightly doped isotropic $t-J$ ladder [15]. Using a DMRG approach, the behavior of $C_S(r-r')$ with the usual BCS bond pair operator,

$$\Delta(i) = c_{i,1;\uparrow}c_{i,2;\downarrow} - c_{i,1;\downarrow}c_{i,2;\uparrow} , \tag{15}$$

can also be obtained directly, leading, in the case of the isotropic $t-J$ model [14], to a good agreement with the ED results. More recently, this study was extended to the anisotropic Hubbard ladder [26] showing a pronounced peak of the long-distance pair correlations as a function of $t_\perp$.

Here, as a complementary study of the analysis presented for the binding energy in the previous Subsection, the behavior of the pair correlation function of the BCS-like operator of equation (15) is compared against the case where a spatially-extended pair operator is used. The first motivation to introduce this new pair operator is due to the structure of the hole pair; indeed, it turns out that configurations in which the two holes sit along the diagonal of a plaquette carry a particularly large weight in the 2-hole GS both in the case of the 2D $t-J$ model [35] or in the case of the $t-J$ ladder [31]. This feature seems counterintuitive in a two-hole bound state of $d_{x^2-y^2}$ character, as it is the case *e.g.* in 2D (for ladders, this symmetry is only approximate), since the pair state is odd with respect to a reflection along the plaquette diagonals. However, it has been observed [36] that retardation provides in fact

a simple physical explanation of this apparent paradox. Secondly, it is clear that pairs extending into a larger region of space can acquire more internal kinetic energy and they are less sensitive to short distance electrostatic repulsion.

To study the influence of the spatial extension of the pair operator $\Delta(r)$ on the pair-pair correlation, following reference [35] here a *plaquette* pair operator is defined as

$$\Delta(i+1/2) = (\mathbf{S}_{i,2} - \mathbf{S}_{i+1,1}) \cdot \mathbf{T}_{i,1;i+1,2} - (\mathbf{S}_{i,1} - \mathbf{S}_{i+1,2}) \cdot \mathbf{T}_{i+1,1;i,2} \qquad (16)$$

where $\mathbf{T}_{i,\alpha;j,\beta} = \frac{1}{i} c_{i,\alpha;\sigma} (\sigma_y \boldsymbol{\sigma})_{\sigma\sigma'} c_{j,\beta;\sigma'}$ is the regular (oriented) spin triplet pair operator [37]. Physically, $\Delta^\dagger(i+1/2)$ creates a singlet pair centered on a plaquette in a $d_{x^2-y^2}$ state with holes located along the diagonals of the plaquette (at distance $\sqrt{2}$). The interpretation of this operator is simple: starting from a hole pair located on a rung, the hopping of one of the holes by one site along the leg-ladder leaves behind a spin with the opposite orientation than the local AF pattern. This argument naturally leads to a 3-body problem [36] involving a triplet hole pair and a local spin flip (of triplet character). Formally, this picture is equivalent to introducing some retardation in the usual BCS operator *i.e.* the two holes can be created at two different times separated by an amount τ *e.g.* by applying $c_{i,1;\uparrow}(\tau/2) c_{i,2;\downarrow}(-\tau/2)$ on the AF background. The expansion of this new operator to order τ^2 then leads to the various terms of equation (16). Alternatively, $\Delta^\dagger(i+1/2)$ can also be viewed as the simplest $d_{x^2-y^2}$ operator of global singlet character creating a pair on the diagonals of a plaquette. This result can be deduced from simple symmetry considerations [35].

Our results for $C_s(r)$ in the case of the rung BCS-like operator are shown in Figures 9a, 9b for the Hubbard and $t-J$ ladders, respectively. Both sets of data are consistent with the power law decay and show a clear increase of the correlations at intermediate distances. In the case of the $t-J$ ladder at $n = 0.75$, the maximum occurs for $t_\perp \simeq 1.5$, a value slightly larger than the characteristic value corresponding to the maximum of Δ_B. According to Figures 2 and 5 showing the single particle spectral functions for almost identical parameters, this specific value of $t_\perp$ seems to correspond to the case where the chemical potential sits in the vicinity of a maximum of the density of states generated by very flat bands at the band edge (as suggested in Ref. [26] and in agreement with the general ideas discussed in Ref. [38]). On the other hand, it is likely that the maximum of Δ_B does not occur at exactly the same value of $t_\perp$ but rather at a somewhat smaller value.

The plaquette pair-pair correlations are shown in Figure 9c. At short distance $r = 1$, the correlations are suppressed reflecting the spatial extension of the pair operator. At larger distances, $r \geq 2$, a significant overall increase is observed compared to the case of the rung operator, showing that indeed the use of "extended" operators to capture the usually weak signals of superconductivity in doped antiferromagnetic systems is a promising strategy [39]. Note that, apart from this overall factor, the functional form of the decay seems to be identical

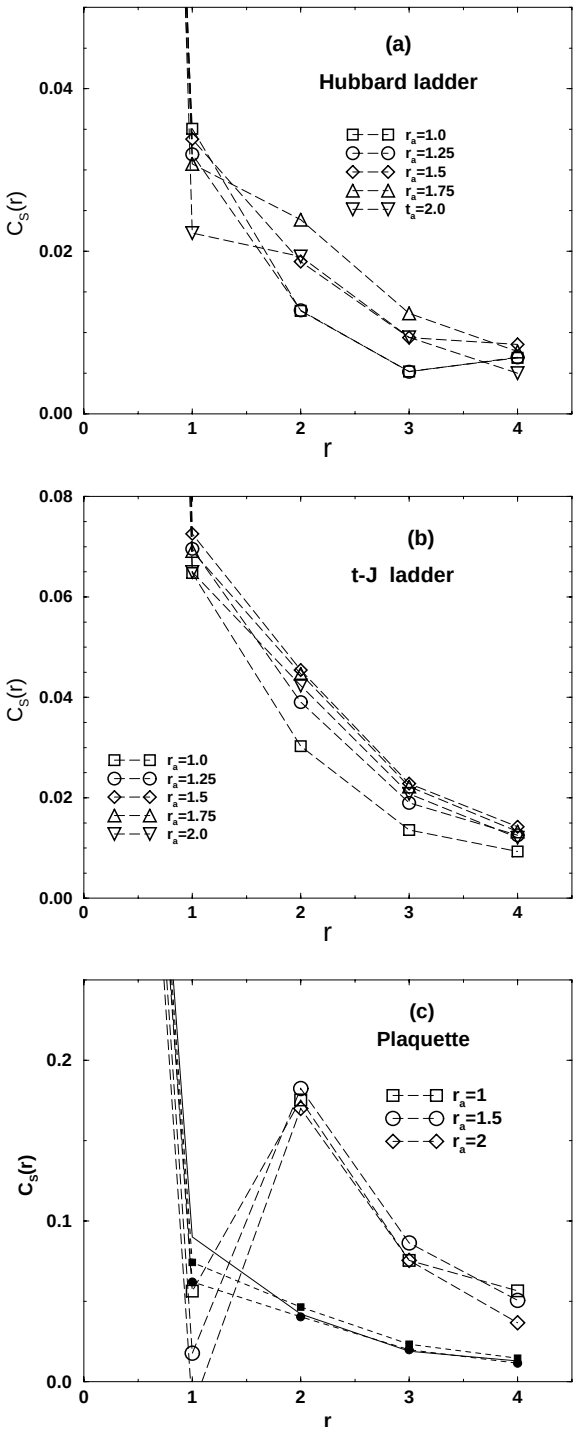

Fig. 9. Pair-pair correlation function *versus* distance calculated on 2×8 clusters at density $n = 0.75$ with PBC in the chain direction. The values of the anisotropy $r_a = t_\perp/t_\parallel$ are indicated on the plot. (a) rung-rung correlations in the Hubbard ladder for $U = 10$; (b) rung-rung correlations in the $t-J$ ladder for $J_\parallel = 0.4$; (c) plaquette-plaquette correlations (open symbols) in the $t-J$ ladder for $J_\parallel = 0.4$. For comparison, some of the correlations of the rung pair operator of (b) are also reproduced (small full symbols) on the same plot.

to the one obtained for the rung operator (as can be checked quantitatively).

It is interesting to compare the previous results of the pair-pair correlations with the (rung) density-density correlations,

$$C_D(r-r') = \left\langle \rho(r)\rho(r') \right\rangle_0 , \tag{17}$$

which, according to conformal invariance, is expected to follow in the $C1S0$ phase a power law behavior of the form

$$C_D(r-r') \sim \frac{\cos\left(4k_F(r-r')\right)}{|r-r'|^{2K_\rho}} \ . \tag{18}$$

The relationship between the two exponents characterising the power law behaviors (14, 18) reflects the competition between $4k_F$-CDW and SC fluctuations. As shown in Figure 10 the density-density correlations show a pronounced maximum at distance 4 which corresponds to the occurrence of strong short range $4k_F$ charge correlations in agreement with (18). In other words, the pairs tend to form, at short distances, a charge density wave with a wave vector $\lambda_{4k_F}/a = 1/n_h$ ($= 4$ in this case). However, our cluster sizes are not large enough to observe the algebraic decay of the charge correlations at longer distances.

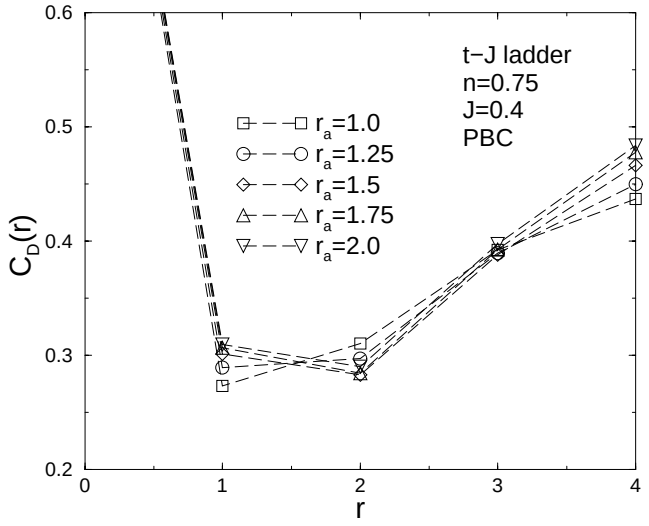

Fig. 10. Density-density correlation function of the $t-J$ ladder $J_\parallel = 0.4$ *versus* distance calculated on 2×8 clusters at density $n = 0.75$ and $J_\parallel = 0.4$. PBC in the chain direction are used. The values of the anisotropy $r_a = t_\perp/t_\parallel$ are indicated on the plot.

We finish this section by a brief discussion on the connection of this work to the experiments on the doped $Sr_{14-x}Ca_xCu_{24}O_{41}$ ladder material [10]. A fairly good description of the ambient pressure transport and NMR properties of this material in term of an isolated ladder (with $r_a \sim 0.5$) seems appropriate. Indeed, the resistivity in the direction of the ladders shows a clear metallic behavior while some localization is seen perpendicular to the ladders. This phenomenum can be interpreted by the formation of pairs in the ladder (also compatible with the opening of a spin gap as seen in NMR) hence reducing single particle tunneling across the ladders. In this picture, no 3D coherence is established although individual pairs exist as expected in our model. In addition, the localization observed at lower temperature in the ladder direction can be attributed to a pinned $4k_F$-CDW. The exact nature of the SC phase under pressure is, on the other hand, not resolved. Indeed, at $P \simeq 30$ kbar, the resistivity becomes much less anisotropic and NMR measurements suggest that the spin gap disappears above the superconducting transition temperature [10]. Therefore, it is not clear yet whether this SC phase corresponds to the 3D ordering of the dominant ladder pair-pair fluctuations by Josephson coupling.

4 Conclusions

In this paper dynamical properties of anisotropic ladders have been investigated using the one-band Hubbard and $t-J$ models. An analysis based on the local-rung approximation explains a considerable part of the numerical results. In particular, the existence of a metal-insulator transition at quarter filling which can be justified in such an analysis was indeed numerically seen for increasing anisotropy ratio. Flat quasiparticle dispersions at the chemical potential are observed in regions of parameter space where pairing correlations are robust. A finite-size scaling of the binding energy and the spin-gap show that these quantities change with the anisotropy ratio in a manner similar as the pair correlations do. In agreement with previous results, it is observed that superconducting correlations are maximized for anisotropic systems, with couplings along rungs slightly larger than along the legs.

E. D. is supported by the NSF grant DMR-9520776. D.P. and J.R. thank IDRIS, Orsay (France) for allocation of CPU time on the C94, C98 and T3E Cray supercomputers. J.R. acknowledges partial support from the Ministry of Education (France) and the "Centre National de la Recherche Scientifique" (CNRS).

References

1. For a review see *e.g.* E. Dagotto, T.M. Rice, Science **271**, 618 (1996).
2. M. Uehara, T. Nagata, J. Akimitsu, H. Takahashi, N. Môri, K. Kinoshita, J. Phys. Soc. Japan. **65**, 2764 (1996).
3. P. Millet *et al.*, Phys. Rev. B **57**, 5005 (1998).
4. H. Smolinski, C. Gros, W. Weber, U. Peuchert, G. Roth, M. Weiden, C. Geibel, cond-mat/9801276 (1998).
5. H. J. Schulz, Phys. Rev. B **34**, 6372 (1986).
6. E. Dagotto, A. Moreo, Phys. Rev. B **38**, 5087 (1988); E. Dagotto, J. Riera, D.J. Scalapino, Phys. Rev. B **45**, 5744 (1992).
7. M. Azuma, Z. Hiroi, M. Takano, K. Ishida, Y. Kitaoka, Phys. Rev. Lett. **73**, 3463 (1994).

8. Z. Hiroi, M. Takano, Nature **377**, 41 (1995).
9. M. Sigrist, T.M. Rice, F.C. Zhang, Phys. Rev. B **49**,12058 (1994); H. Tsunetsugu, M. Troyer, T.M. Rice, Phys. Rev. B **49**,16078 (1994).
10. A. Mayaffre *et al.*, Science **279**, 345 (1998) and references therein.
11. D. Poilblanc, D. J. Scalapino, W. Hanke, Phys. Rev. B **52**, 6796 (1995).
12. A.M. Finkel'stein, A.I. Larkin, Phys. Rev. B **47**, 10461 (1993); M. Fabrizio, Phys. Rev. B **48**, 15838 (1993); N. Nagaosa, Solid State Commun. **94**, 495 (1995).
13. L. Balents, M.P.A. Fisher, Phys. Rev. B **53** 12133 (1996); H.J. Schulz, Phys. Rev. B **54** R2959 (1996).
14. C. Hayward, D. Poilblanc, R.M. Noack, D.J. Scalapino, W. Hanke, Phys. Rev. Lett. **75**, 926 (1995).
15. C. Hayward, D. Poilblanc, Phys. Rev. B **53**, 11721 (1996). See also H. Tsunetsugu, M. Troyer, T.M. Rice, Phys. Rev. B **51**, 16456 (1995).
16. To distinguish the different phases, the notation $CnSm$ was introduced in reference [13] to label a phase with n gapless charge modes and m gapless spin modes.
17. E. Orignac, T. Giamarchi, Phys. Rev. B **56**, 7167 (1997).
18. T.F. Müller, T.M. Rice, Phys. Rev. B **58**, 3425 (1998).
19. R.S. Eccleston, M. Uehara, J. Akimitsu, H. Eisaki, N. Motoyama, S. Uchida, cond-mat/9711053 (1997).
20. D.C. Johnston, Phys. Rev. B **54**, 13009 (1996).
21. P. Horsch, F. Mack, cond-mat/9801316 (1998).
22. D. Augier, D. Poilblanc, S. Haas, A. Delia, E. Dagotto, Phys. Rev. B **56**, R5732 (1997).
23. T. Barnes, E. Dagotto, J. Riera, E. Swanson, Phys. Rev. B **47**, 3196 (1993); see also S. Gopolan, T.M. Rice, M. Sigrist, Phys. Rev. B **49**, 8901 (1994).
24. H. Endres, R.M. Noack, W. Hanke, D. Poilblanc, D.J. Scalapino, Phys. Rev. B **53**, 5530 (1996).
25. C. Kim, A.Y. Matsuura, Z.-X. Shen, N. Motoyama, H. Eisaki, S. Uchida, T. Tohyama, S. Maekawa, Phys. Rev. Lett. **77**, 4054 (1996); C. Kim *et al.*, Phys. Rev. B **56**, 15589 (1997).
26. R.M. Noack, N. Bulut, D.J. Scalapino, M.G. Zacher, Phys. Rev. B **56**, 7162 (1997).
27. E. Dagotto, G.B. Martins, J. Riera, A.L. Malvezzi, C. Gazza, Phys. Rev. B **58**, 12063 (1998).
28. G. Martins, J. Riera, E. Dagotto, unpublished.
29. In this case, one cannot completely exclude an exponentially small single particle gap.
30. Calculations of $A(\mathbf{q},\omega)$ in the *isotropic* $t-J$ ladder can be found *e.g.* in S. Haas, E. Dagotto, Phys. Rev. B **54**, R3718 (1996).
31. S. White, D.J. Scalapino, Phys. Rev. B **55**, 6504 (1997).
32. C. Gazza *et al.*, preprint (cond-mat/9803314).
33. M. Reigrotzki, H. Tsunetsugu, T.M. Rice, J. Phys. C **6**, 9235 (1994).
34. M. Greven, R.J. Birgeneau, U.-J. Wiese, Phys. Rev. Lett. **77**, 1865 (1996).
35. D. Poilblanc, Phys. Rev. B **49**, 1477 (1994).
36. J. Riera, E. Dagotto, Phys. Rev. B **57**, 8609 (1998).
37. D.P. thanks D.J. Scalapino for pointing out a misprint in note [21] of reference [35]. The correct expression for $\mathbf{S}_k \cdot \mathbf{T}_{i;j}$ reads $S^Z_k\,(c_{i;\uparrow}c_{j;\downarrow} - c_{j;\uparrow}c_{i;\downarrow}) - S^+_k\,c_{i;\uparrow}c_{j;\uparrow} + S^-_k\,c_{i;\downarrow}c_{j;\downarrow}$.
38. E. Dagotto, A. Nazarenko, A. Moreo, Phys. Rev. Lett. **74**, 310 (1995).
39. Related ideas where presented years ago in the same context by E. Dagotto, J.R. Schrieffer, Phys. Rev. **B 43**, 8705 (1991).